



1 Modelling groundwater recharge, actual evaporation and 2 transpiration in semi-arid sites of the Lake Chad Basin: The role of 3 soil and vegetation on groundwater recharge

4 Christoph Neukum¹, Angela Gabriela Morales Santos², Melanie Ronelngar³, Aminu Bala⁴, Sara Ines
5 Vassolo¹

6 ¹ Federal Institute for Geosciences and Natural Resources, Department of Groundwater and Soil, Stilleweg 2, 30655 Hannover,
7 Germany

8 ² University of Natural Resources and Life Sciences, Vienna, Department of Water, Atmosphere and Environment, Institute
9 for Soil Physics and Rural Water Management, Muthgasse 18, 1190 Vienna, Austria

10 ³ Federal Institute for Geosciences and Natural Resources at Lake Chad Basin Commission, Rond Point des Armes, Ndjamen
11 Chad

12 ⁴ Lake Chad Basin Commission, Rond Point des Armes, Ndjamen, Chad

13 *Correspondence to:* Christoph Neukum (christoph.neukum@bgr.de)

14 Abstract

15 The Lake Chad Basin, located in the center of North Africa, is characterized by strong climate seasonality with a pronounced
16 short annual precipitation period and high potential evapotranspiration. Groundwater is an essential source for drinking water
17 supply as well as for agriculture and groundwater related ecosystems. Thus, assessment of groundwater recharge is very
18 important although difficult, because of the strong effects of evaporation and transpiration as well as limited available data.

19 A simple, generalized approach, which requires only limited field data, freely available remote sensing data as well as well-
20 established concepts and models, is tested for assessing groundwater recharge in the southern part of the basin. This work uses
21 the FAO-dual K_c concept to estimate E and T coefficients at six locations that differ in soil texture, climate, and vegetation
22 conditions. Measured values of soil water content and chloride concentrations along vertical soil profiles together with different
23 scenarios for E and T partitioning and a Bayesian calibration approach are used to numerically simulate water flow and chloride
24 transport using Hydrus-1D. Average groundwater recharge rates and the associated model uncertainty at the six locations are
25 assessed for the 2003-2016 time-period.

26 Annual groundwater recharge varies between 6 and 93 mm and depends strongly on soil texture and related water retention
27 and on vegetation. Interannual variability of groundwater recharge is generally greater than the uncertainty of the simulated
28 groundwater recharge.

29 1 Introduction

30 The Lake Chad Basin (LCB) is one of the largest endorheic basins of the world with an area of approximately 2.5 million km².
31 The basin covers parts of Algeria, Cameroon, Central African Republic, Chad, Libya, Niger, Nigeria, and Sudan. According
32 to the Lake Chad Basin Commission (LCBC, 2012), 45 million inhabitants are settled in the basin. The study areas of Salamat



33 and Waza Logone are located in the southern part of the LCB along the Chari-Logone, the major tributary river system to Lake
34 Chad (Figure 1), which accounts for around 80-90% of the inflow to the Lake Chad (Bouchez et al., 2016).

35 Groundwater is an important source for drinking water supply as well as for agriculture and groundwater related ecosystems
36 in the LCB. Lake Chad, associated rivers, and the floodplains of the major rivers are characterized by strong seasonality, due
37 to a pronounced short annual precipitation period and high potential evapotranspiration. Groundwater recharge, evaporation,
38 transpiration, and the entire hydrological budget depend strongly on seasonality. However, the impact of transpiration as a
39 potentially significant process of the hydrological budget (Jasechko et al., 2013) has not yet been intensively explored in the
40 area (Bouchez et al., 2016).

41 Many studies have been published concerning the hydrological behaviour and budget of Lake Chad, due to its substantial and
42 frequent open water surface changes and related consequences to the population and the environment (e.g. Bouchez et al.,
43 2016; Lemoalle et al., 2012; Olivry et al., 1996; Vuillaume, 1981). Another important topic associated to Lake Chad is
44 groundwater recharge by infiltration of lake water into the Quaternary aquifer, which was estimated by isotope studies (Fontes
45 et al., 1969; Fontes et al., 1970; Gaultier, 2004; Zairi, 2008), water and salt budgets (Bader et al., 2011; Carmouze, 1972;
46 Roche, 1980) and hydrogeological models (Isihoro et al., 1996; Leblanc, 2002). Local scale studies focusing on the
47 hydrological processes in the vadose zone are largely missing in the LCB. Recently Tewolde et al. (2019) published such a
48 study using stable isotope and chloride concentrations in some of the same soil profiles used in this work.

49 For vadose zone studies, partitioning evapotranspiration (ET) into its respective soil evaporation (E) and plant transpiration
50 (T) components is crucial for process-based understanding of fluxes (Anderson et al., 2017). There are a number of
51 measurement and modelling approaches that can be used to estimate E and T separately, including micro-lysimeters, soil heat
52 pulse probes, Bowen ratios, and Eddy covariance to determine E, and sap flow, chambers, and biomass-transpiration
53 relationships to measure T (Kool et al., 2014). Evapotranspiration partitioning can also be estimated directly by using stable
54 isotopes to assess the ratio between E and T (Wu et al. 2016). Stable isotopes were also used in combination with Eddy
55 covariance on semi-arid environments (Aouade et al., 2016).

56 The Food and Agricultural Organization of the United Nations (FAO) published a model (Allen et al., 1998) that uses an
57 empirically defined crop coefficient (K_c) in combination with a grass-reference potential ET (ET_0) to calculate crop potential
58 evapotranspiration (ET_c). There are two approaches for this method: single coefficient and dual crop coefficient. The FAO-
59 dual K_c model is a validated method for ET partitioning and the most commonly applied (Kool et al., 2014). It has been widely
60 used with good results for numerous crops under different conditions: e.g. wheat and maize in semi-arid regions (Shahrokhnia
61 and Sepaskhah, 2013), wheat in humid climates (Vieira et al., 2016), cherry trees in temperate continental monsoon climates
62 (Tong et al., 2016), and irrigated eucalyptus (Alves et al., 2013) and canola in terrestrial climates (Majnooni-Heris et al., 2012).
63 Quantification of water fluxes in the vadose zone and linking atmospheric water and solute input at the upper boundary of the
64 soil with water and solute fluxes at different soil depths is frequently implemented using different type of models. Numerical
65 models need information on vadose zone properties for accurate parametrization to link fluxes with state variables such as
66 unsaturated hydraulic conductivity and the water retention curve. Estimation of effective soil hydraulic parameters, which are



67 valid at the modelling scale, might be laborious. Furthermore, parameter estimation might vary significantly depending on the
68 measurement method (Mertens et al., 2005), when water and solute fluxes dynamics are considered. Hydraulic and transport
69 parameters obtained from inverse modelling can be ambiguous, if multiple parameters are simultaneously considered and
70 boundary conditions are not well known. Combining different state variables of water flow and solute transport in one objective
71 function was found to be a useful strategy for appropriate parametrization (Groh et al., 2018; Sprenger et al., 2015) and for the
72 transient simulation of water and solute fluxes. However, large amount of data are necessary to obtain accurate estimates of
73 state variables, which are rarely available in remote areas of Africa, and measurement of related variables are associated with
74 a huge effort in such environments. Pedotransfer functions (PTF) bridge available and needed data and are frequently used to
75 quantify soil parameters (van Looy et al., 2017; Vereecken et al., 2016). PTF strive to provide a balance between data accuracy
76 and availability (Vereecken et al., 2016). Since PTF usually do not consider soil structure, their results are better for
77 homogeneous soils than for structured ones (Sprenger et al., 2015; Vereecken et al., 2010).

78 Recharge occurs even in the most arid regions, mainly due to concentration of surface flow and ponding with lateral and
79 vertical infiltration (Lloyd, 1986). Direct recharge by precipitation is possible in semi-arid regions, but intermittently, owing
80 to the fluctuations in the periodicity and volume of precipitation that is inherent to such regions (Lloyd, 2009). Scanlon et al.
81 (2006) synthesized recharge estimates for semiarid and arid regions globally. They found that recharge is sensitive to land use
82 and cover changes, hence management of such changes are necessary to control recharge. Moreover, they stated that average
83 recharge rates in semi-arid and arid regions range from 0.2 to 35 mm yr⁻¹, representing 0.1 to 5% of long-term average annual
84 precipitation. Edmunds et al. (2002) estimated direct recharge rates from precipitation in the Manga Grasslands in NE Nigeria
85 (western LCB) at rates between 16 mm year⁻¹ and 30 mm yr⁻¹. Using the same method, they appraised the regional direct
86 recharge for north Nigeria at 43 mm year⁻¹, which highlights the importance of infiltration from precipitation to the
87 groundwater table at the regional scale. Recently, Cuthbert et al. (2019) investigated the relationship between precipitation and
88 recharge in sub-Saharan Africa using multidecadal hydrographs. They found that focused recharge predominates in arid areas
89 and is mainly controlled by intense rainfall and flooding events. Intense precipitation, even during years of lower annual
90 precipitation, results in some of the most significant years of recharge in dry subtropical locations.

91 The Chloride Mass Balance (CMB) approach is a widely used technique for estimating groundwater recharge. Edmunds and
92 Gaye (1994) used interstitial water chloride profiles from the unsaturated zone, in combination with measurements of chemical
93 parameters from dug well samples, to calculate groundwater recharge in the Sahel (where the mean annual rainfall from 1970-
94 1990 was around 280 mm). A recharge rate of 13 mm year⁻¹ over the studied area was obtained. They conclude that it is an
95 inexpensive technique, which can be applied in many arid and semi-arid areas. Tewelde et al. (2019) applied the CMB on soil
96 profiles of the LCB, which are partly used in this study. They estimated generally lower annual recharge in Salamat (3 to 19
97 mm year⁻¹) compared to Waza Logone (50 to 118 mm year⁻¹). One major difficulty of CMB is the choice of a representative
98 chloride concentration, or the concentration that prevails at greater depths, when evapotranspiration effects are negligible,
99 particularly for soils with a strong vertical variability in chloride concentrations.



100 In general, time series of relevant data for estimating groundwater recharge is scarce in the LCB. A simple, generalized
101 approach, which requires only limited field data, freely available remote sensing data, and well-established concepts and
102 models, is tested for assessing groundwater recharge in the semi-arid part of the LCB. This work applies the FAO-dual K_c
103 concept to estimate E and T coefficients at six locations, which differ in soil texture, climate, and vegetation conditions.
104 Measured values of soil water content and chloride concentrations along vertical soil profiles, partly published by Tewelde et
105 al. (2019), together with different scenarios for E and T partitioning and a Bayesian calibration approach are used to
106 numerically simulate water flow and chloride transport as well as to produce time series of recharge. Average potential
107 groundwater recharge and the associated model uncertainty are assessed for the 2003-2016 time-period. The manuscript
108 demonstrates that this simple and well-known approach also provides reliable estimations on groundwater recharge for areas
109 with scarce data availability, which is a key issue in arid regions.

110 **2 Data and methods**

111 **2.1 Study sites**

112 The LCB is a Mesozoic basin and a major part of its geology comprises sedimentary formations from the Tertiary and
113 Quaternary periods (LCBC, 1993). The Quaternary sediments form a continuous layer of fluvial, lacustrine and aeolian
114 sands. These medium to fine-grained sands act as an unconfined transboundary aquifer, as do all aquifers in the LCB, and are
115 isolated from underlying aquifers by a thick layer of Pliocene clay (Leblanc et al., 2007; Vassolo, 2009). The Tertiary formation
116 (Continental Terminal) consists of sandstones and argillaceous sands and is a classic example of a confined aquifer system
117 that becomes artesian in the surroundings of Lake Chad (Ngatcha et al., 2008). The availability of water from precipitation as
118 well as the deposition characteristics of the aquifer play an important role in the recharge of the upper unconfined sands
119 (Vassolo, 2009).

120 The study sites (Figure 1, Table 1) are located in the Salamat and Waza Logone floodplains in the southern Sahel zone and
121 correspond to those published by Tewelde et al. (2019) for these areas, except for site ST4. Site ST4 is located far from any
122 floodplain, which is the focus of this research, and its soil composition and vegetation are very similar to those from site ST3.
123 Thus, including this location would not provide any additional information.

124 Sites ST1 and ST2 in Salamat as well as WL1 and WL3 in Waza Logone are annually flooded over three months, site WL2
125 located at the edge of the Waza Logone wetland is flooded only one month per year whereas site ST3, although close to ST1
126 in Salamat, is never flooded. In the Salamat region, mainly sorghum is grown with trees such as *Acacia albida*, *A. scorpioides*
127 and *A. sieberana*, present along the margins of the floodplains (Bernacsek et al., 1992). In the Waza Logone area, vegetation
128 depends on the duration of submersion, forming grass savannahs that are flooded for longer periods of time (Batello et al.,
129 2004).



130 2.2 Climate data

131 Monthly precipitation and potential evapotranspiration data from 1970 to 2019 for the study sites were extracted from the
132 CRUTS 4 database (Harris et al., 2020). The potential evapotranspiration was calculated using the Penman-Monteith method
133 and is considered herein as the reference evapotranspiration (ET_0). Wind speeds at 10 m above ground for Salamat and Waza
134 Logone were obtained from Didane et al. (2017). To adjust these values for 2 m above ground, a correction factor of 0.7479
135 was applied, based on a logarithmic wind speed profile (Allen et al., 1998).

136 Average annual precipitation in Salamat and Waza Logone are 807 mm and 709 mm, respectively. The rainy season is typically
137 from May to September with maximum precipitation in July and August. Average annual values of ET_0 are 1718 mm in
138 Salamat and 2011 mm in Waza Logone, exceeding annual precipitation by more than a factor of 2. However, in the second
139 half of the rainy season, the monthly water balance is positive. The average water balance for July until September between
140 2003 and 2016 was $131 \pm 101 \text{ mm month}^{-1}$ and $90 \pm 63 \text{ mm month}^{-1}$ for Salamat and Waza Logone, respectively (Figure 2).

141 Chloride concentration was analyzed in the BGR laboratory in Hanover, Germany using a Thermo Fischer (Dionex) type ICS-
142 5000 ion chromatograph with a detection limit of 0.003 mg l^{-1} . Concentration in ponding water was measured in four samples
143 in Salamat, which varied between 2.5 mg l^{-1} and 25 mg l^{-1} .

144 Precipitation was sampled using a Hellmann rainwater collector in N'Djamena. This device was designed to minimize to a
145 minimum evaporation by using a narrow soft polypropylene plastic tube of 4 mm inner diameter to connect the funnel on top
146 of the device with the bottom of the 3 l collection bottle (Gröning et al., 2012). Once precipitation starts, water rises in the
147 bottle and into the tube decoupling the atmosphere from the bottle headspace to prevent evaporation. To ensure that evaporation
148 is as low as possible, sampling took place event-wise. Chloride concentration in precipitation was measured in 59 out of 147
149 samples collected in N'Djamena between 2014 and 2020 for different precipitation events and stages of the rainy season (Table
150 S1). Not all rain samples could be analyzed for chloride concentration, due to limited sample volume in minor events at the
151 beginning and end of the rainy season.

152 Average chloride concentration in May was $2.5 \pm 2.3 \text{ mg l}^{-1}$ (3 samples). Precipitation in June to September has relatively low
153 chloride concentrations, declining from $0.6 \pm 0.3 \text{ mg l}^{-1}$ to $0.26 \pm 0.12 \text{ mg l}^{-1}$ and $0.38 \pm 0.14 \text{ mg l}^{-1}$ at the end of the season.
154 Strong rain events in July and August have chloride concentrations between 0.2 and 0.3 mg l^{-1} . The annual wet chloride
155 deposition sums to $1.8 \pm 0.5 \text{ kg ha}^{-1}$. The measured values are in the range of published data (Goni et al., 2001; Laouali et al.,
156 2012; Gebru and Tesfahunegn, 2019). Dry deposition of chloride is estimated between 10 – 30% of wet deposition (Bouchez
157 et al. 2019).

158 2.3 Soil and vegetation data

159 At each study site, vertical soil profiles were core-drilled using a hand auger. In Salamat, soil profiles were sampled in 2016
160 (Tewelde et al., 2019) and 2019. In Waza Logone, soil samples were sampled in 2017 only (Tewelde et al., 2019), due to



161 security reasons in 2019. Each of the soil profiles was sampled in 10 cm intervals and filled into headspace glass vials and
162 plastic bags.

163 Each soil fraction was tested for grain size distribution using standard sieving and sedimentation procedures (Tewolde, 2017).

164 Classification follows the soil texture triangle by the US Department of Agriculture (Šimůnek et al., 2011).

165 Chloride concentration was analyzed after aqueous extraction from oven dried (105°C for 24 hours) soil samples following
166 the standard guideline DIN EN 12457-1 (Tewolde, 2017). Data are presented in Tables S2 and S3.

167 Gravimetric water content is the mass of water contained in a sample as a percentage of the dried soil mass. It was obtained
168 by weighing the moist sample, oven drying it at 105°C for 24 to 48 hours, and weighing it again (Tables S2 and S3). Since
169 bulk densities were not measured in the field, volumetric water contents were obtained by multiplying the gravimetric water
170 contents for each soil type and location by typical bulk densities obtained from the Global Gridded Surfaces of Selected Soil
171 Characteristics database (Global Soil Data Task Group, 2000).

172 The type of vegetation and the annual cycle of crops, length of the flooding period, and vegetation throughout the dry period
173 were mapped during field work and documented by surveying resident populations. In addition, MODIS vegetation indices
174 data (Didan, 2015) were used to justify the documented annual cycle of phenology (Figure 3).

175 **3 Modelling methodology**

176 Our approach assumes that groundwater recharge is controlled by precipitation, evaporation, and transpiration (surface runoff
177 can be neglected due to the flat topography). Soil moisture and chloride concentration along the soil profile at a certain time
178 are indicators for evaporation and transpiration processes within the root zone of soils. Chloride concentration in soil depends
179 on its input via precipitation and washing out of dry deposition as well as on the amount of evaporation and transpiration on
180 the soil surface and in the root zone.

181 The first estimation of evapotranspiration was carried out using the FAO-dual crop coefficient approach that assesses E and T
182 individually. The uncertainty of E and T partitioning on soil water and chloride concentration in the six soil profiles was
183 assessed by considering scenarios of mean, maximum, and minimum E and T coefficients (see 3.1). Calculated time series of
184 E and T for the site-specific vegetation were used to estimate soil water and chloride concentration profiles at the sampling
185 time in each of the six locations using Hydrus-1D. A Bayesian approach was applied to consider uncertainties in chloride
186 concentrations of precipitation and dry deposition, in partitioning E and T as well as in the parametrisation of the soil hydraulic
187 model (Figure 4).

188 **3.1 Partitioning of evaporation and transpiration**

189 Evapotranspiration (ET) is the combination of two main processes driven by atmospheric demand: evaporation from the soil
190 (E) and transpiration through the stomata of plants (T) and is an important component of the water balance, especially in semi-
191 arid areas. The FAO provides a model (Allen et al., 1998) for estimating crop evaporation (ET_c) based on an empirically



192 defined crop coefficient (K_c) combined with a reference evapotranspiration (ET_0). Two approaches are possible, single crop
193 coefficient and dual crop coefficient. The latter was applied in this work.

194 The dual K_c method (Allen et al., 1998) is the sum of two coefficients, the basal crop coefficient (K_{cb}) that describes plant
195 transpiration and the soil water evaporation coefficient (K_e) that depicts evaporation from the soil surface. K_{cb} is defined as
196 the ratio of crop evapotranspiration over reference evapotranspiration (ET_c/ET_0), when the soil surface is dry and transpiration
197 occurs at a potential rate (i.e. unlimited water availability for transpiration). K_e is highest when the topsoil is wet, but
198 diminishes with drying out of topsoil to become zero, if no water remains near the soil surface for evaporation.

199 The parameters required for the estimation of monthly ET_c are the monthly reference evapotranspiration (ET_0), the monthly
200 basal crop coefficient (K_{cb}) and the monthly soil water evaporation coefficient (K_e):

$$201 \quad ET_c = ET_0 * K_c = ET_0 * (K_{cb} + K_e), \quad (2)$$

202 Onsite information on vegetation and phenology, such as month of planting, full emergence of crops, and harvesting times,
203 was used to define the monthly variation of vegetation at the study sites. These different vegetation periods were combined
204 with crop-specific K_{cb} values for sorghum and grass provided in Allen et al. (1998) for a sub-humid climate with relative
205 humidity of 45% and an average moderate wind speed of 2 m s^{-1} . To comply with the local semi-arid climate conditions in
206 Salamat and Waza Lagone, the coefficients K_{cb} for mid- and late-time vegetation periods were adjusted as proposed by Allen
207 et al. (1998). Monthly K_{cb} values for Acacia were estimated based on Do and Rocheteau (2003) and Do et al. (2008). Site-
208 specific monthly variation of ground cover and flooding periods with ranges of crop coefficient (K_{cb}), soil water evaporation
209 coefficient (K_e), and root depth are provided in Table S4.

210 **3.2 Modelling water flow and solute transport**

211 **3.2.1 Model concept, setup, and initial conditions**

212 The chloride profiles measured in soil at a certain time represent water and solute budget input from past precipitation events
213 and can be estimated by transient water flow and solute transport modelling. The model concept assumes that atmospheric
214 chloride input is restricted to solute in precipitation and that the chloride concentration profile results from solute enrichment
215 in the soil, due to evaporation and transpiration. An accurate parametrization of the unsaturated flow and transport model as
216 well as a robust quantification of groundwater recharge are not possible with the available data and hence cannot be included
217 within the scope of this study. However, the model results estimate groundwater recharge magnitude and variability based on
218 information regarding soil texture and vegetation as well as associated uncertainty in results. This proposed approach is
219 appropriate for locations with limited availability of long-term soil water measurements.

220 The free software package Hydrus-1D version 4.17.0140 was used to simulate transient water flow and solute transport in the
221 six variably saturated soil profiles. Hydrus-1D numerically solves the Richards (1931) equation for variably saturated water
222 flow, advection-dispersion equations for heat, and solute transport (Šimůnek et. al, 2009):

$$223 \quad \frac{\partial \theta(h)}{\partial t} = \frac{\partial}{\partial z} \left[K(h) \left(\frac{\partial h}{\partial z} + \cos \alpha \right) \right] - S(h) \quad (3)$$



224 with:
225 h soil water pressure head [L]
226 θ volumetric water content [L^3L^{-3}]
227 t time [T]
228 z spatial coordinate [L] (positive upwards)
229 S sink term [$L^3L^{-3}L^{-1}$]
230 α angle between flow direction and vertical axis
231 $K(h)$ unsaturated hydraulic conductivity function [LT^{-1}]

232

233 The processes simulated at the six study sites were water flow, solute transport, and root water uptake. Hydrus-1D requires
234 input data at daily time steps, but available precipitation and evaporation data were monthly. Daily values were calculated
235 dividing monthly data by month-specific days. Thus, all days in a month had the same precipitation rate and the same
236 evapotranspiration rate. Model execution ended at the soil sampling time (December 2016 and July 2019 for Salamat and June
237 2017 for Waza Logone). Progressive root growth was considered in all profiles except for ST2, in which the roots of the Acacia
238 trees were distributed along the whole profile and assumed invariant over the simulation period. Since initial conditions of soil
239 moisture and resident chloride concentration are unknown, arbitrary values were adopted. To account for different residence
240 times of water and chloride, due to different degrees of evapotranspiration and unknown initial conditions, each model was
241 run over a period of time long enough to allow the exchange of at least one water column volume. Thus, total modelling periods
242 are different depending on the soil type at each site: ST1, ST2 start in 1910, ST3 in 2010, WL1 and WL2 in 1990, and WL3
243 in 1970. All profiles were discretized into 101 nodes and different horizons according to the soil types interpreted from the
244 individual grain size distributions.

245 3.2.2 Water flow

246 For calculation of water retention (θ) and unsaturated hydraulic conductivity functions ($K(h)$), the Mualem-van Genuchten
247 (MVG) model (van Genuchten, 1980) was applied:

$$248 \theta(h) = \begin{cases} \theta_r + \frac{\theta_s - \theta_r}{[1 + |ah|]^m} & h < 0 \\ \theta_s & h \geq 0 \end{cases} \quad (4)$$

249

$$250 k(h) = k_s S_e^{-1} \left[1 - (1 - S_e^{1/m})^m \right] \quad (5)$$

251 where:

$$252 m = 1 - \frac{1}{n}; \quad n > 1$$



253
$$S_e = \frac{\theta(h) - \theta_r}{\theta_s - \theta_r}$$

254 with

255 θ water content [$L^3 L^{-3}$]

256 h hydraulic head [L]

257 θ_r residual water content

258 θ_s saturated water content

259 α inverse of the air-entry value, empirical [L^{-1}]

260 n pore-size distribution index, empirical [-]

261 l pore-connectivity parameter, empirical ≈ 0.5 [-]

262 S_e effective saturation [-]

263 k_s saturated hydraulic conductivity [LT^{-1}]

264

265 To reduce computational effort, the initial parametrization of these functions was realized using pedotransfer functions
266 implemented in Rosetta (Schaap et al., 2001), which is a dynamically-linked library coupled to Hydrus-1D. The input
267 parameters for each profile were the percentages of sand, silt, clay, and bulk density at several depths. Whenever consecutive
268 layers of a profile showed almost the same grain size distribution (texture) and soil moisture, the layers were lumped together
269 and parameter averages were used in the model. The tortuosity parameter l [-] of the MVG was set to 0.5 as proposed by
270 Mualem (1976).

271 The upper boundary condition was defined as a variable atmospheric condition, whereas the lower boundary was set to zero-
272 gradient with free drainage of water for all profiles, except WL3 where confined groundwater conditions prevailed below the
273 confining clay layer encountered at 3.9 m depth. During drilling, groundwater was hit at 3.9 m depth, but rapidly rose to 2.6
274 m below surface. Consequently, a constant head condition was implemented at 2.6 m depth.

275 3.2.3 Root water uptake and root growth

276 The sink term (S) in the Richards' equation, defined by Feddes et al. (1978) as the volume of water removed from a unit
277 volume of soil per unit time due to plant water uptake, was considered in all soil profiles according to the prevailing vegetation
278 (Table S4). The Feddes' default parameters for grass were used in the ST3 and Waza Logone profiles. In ST1, where sorghum
279 was planted, Feddes' parameters for corn were used because sorghum is not available in the list. According to Righes (1980)
280 sorghum and corn roots extract water from approximately the same soil depths and have similar average root density
281 distribution.

282 An average root depth of 1 m was adopted in ST1 for the initial and end seasons, and 2 m for development and mid seasons. In
283 the case of Acacia in ST2, the adopted parameters correspond to deciduous trees. The root depth of the Acacia tree was
284 considered as constant over the entire simulation period with maximum root distribution at 0.5 m and decreasing distribution



285 down to 2 m (Beyer et al., 2016). In ST3, the vegetation was defined as grass, while in WL1, WL2 and WL3 it was defined as
286 grass with a flooding period of 3 months in WL1 and WL3, but only one month in WL2. Rooting depth values used at these
287 sites range from 0.1 m to 0.5 m, depending on the growth stage of grass. The median maximum rooting depth value of annual
288 grass in water-limited ecosystems is 0.37 m with a 95% confidence level in an interval of 0.26 m-0.55 m (Schenk and Jackson,
289 2002).

290 **3.2.4 Solute transport**

291 The chloride concentration in soil water was simulated using an equilibrium advection-dispersion model implemented in
292 Hydrus1D. Hydrodynamic dispersion was implemented considering dispersivity values of 1/10th of the individual layer
293 thickness, a molecular diffusion coefficient of $1.3 \times 10^{-9} \text{ m}^2\text{s}^{-1}$, and a tortuosity factor as defined by Millington and Quirk
294 (1961). Adopted dispersivity values are within reported ranges of 0.08 m to 0.20 m (Vanderborght and Vereecken, 2007;
295 Stumpp et al, 2009, 2012).

296 A time-dependent concentration boundary condition was applied to the upper boundary and a zero-gradient boundary condition
297 to the lower boundary. The transient liquid phase concentration of infiltrating rainwater follows measured chloride
298 concentration in precipitation sampled in N'Djamena. The chloride concentration of ponding water correspond to four values
299 measured in Salamat that range from 2.5 mg l^{-1} to 25 mg l^{-1} with an average of 9 mg l^{-1} . Initial chloride concentration in soil
300 water was set to 0 mg l^{-1} . However, each model was run over a period of time long enough to allow the exchange of at least
301 one water column volume (3.2.1). The model does not consider root solute uptake.

302 **3.2.5 Crop evapotranspiration scenario definition**

303 Since crop evapotranspiration was not measured, values were simulated using K_{cb} , K_e , and root depth instead. Because these
304 parameters are given in ranges (Table S4), seven scenarios with different combinations of K_{cb} , K_e , and root depth were
305 developed to assess ranges of crop evaporation (Table 2). Scenario “Mean” corresponds to the average value of all parameters.
306 Scenarios “Min” and “Max” combine the minimum and maximum values, respectively. Scenario “Mix-1” combines minimum
307 K_{cb} with average K_e and root depth, scenario “Mix-2” minimum K_e with average K_{cb} and root depth whereas scenario “Mix-
308 3” combines minimum root depth with average K_e and K_{cb} .

309 **3.2.6 Bayesian model calibration**

310 Based on the crop evapotranspiration scenarios, the models were calibrated and model uncertainty was estimated using a
311 Bayesian calibration. Bayesian analysis is a combination of the data likelihood and the prior distribution using the Bayes
312 theorem (ter Braak and Vrugt, 2008). The sum of likelihood functions for soil moisture and chloride concentration was
313 implemented to calculate the log-likelihood of a simulation given the observations and standard deviations at each calibration
314 step. The posteriori parameter distribution was estimated using the Differential Evolution Markov Chain Monte-Carlo (DE-



315 MCzs) algorithm with three sub-chains (ter Braak and Vrugt, 2008) implemented in the R package BayesianTools (Hartig et
316 al., 2019). The number of iterations was defined individually according to a Gelman-Rubin reduction factor < 1.2 .
317 In the calibration, scaling factors ranging from 0.75 to 1.25 for the MVG parameters (saturated volumetric water content,
318 α , and n) were adopted individually. However, ranges for the MVG model parameter n were constrained to $n > 1.01$. Log-
319 transformed saturated hydraulic conductivity for each layer was considered with ranges from -0.5 to 0.5. The scaling factor
320 for transpiration was simultaneously used as a divisor for evaporation to remain within the calculated rate of ET_0 . From all
321 accepted model runs, 100 were randomly selected at each individual location to evaluate average model results and standard
322 deviations.

323 **4 Results**

324 **4.1 Grain size distribution**

325 Soil textures were defined based on grain size distributions of the six profiles (Figure 5) according to the US Department of
326 Agriculture soil texture triangle. Most profiles are fine-grained soils (clay, sandy clay) and fine-grained soils with intercalation
327 of thin sand and loam layers. Only soil profile ST3 is dominated by sand and sandy clay loam.

328 **4.2 Model parametrization**

329 The calibrated parametrization of the MVG model for each layer of the six sampling locations is plausible (Table 3). The
330 posterior distributions of the Bayesian calibration show the sensitive parameters of the model fit. For ST1, these are n , θ_s ,
331 chloride concentration, and the transpiration fraction in evapotranspiration (T), but the k_s is less sensitive (Fig. S1). For ST2,
332 the sensitivities of the model parameters are similar with k_s of the upper layer being the most sensitive and chloride
333 concentration the least sensitive (Fig. S2). The model fits of the data from site ST3 are generally insensitive. Only α , n , and k_s
334 of the upper layer as well as chloride concentration show tighter posteriori distributions (Fig. S3). For site WL1, the model
335 parameters n of layers 1, 2, and 3 as well as the saturated water content of layers 3 and 5, and subordinately of layer 4, are
336 sensitive (Fig. S4). For WL2, the model parameters n of all layers, k_s of layer 3, and θ_s of layers 2 and 3 are sensitive (Fig.
337 S5). For WL3, θ_s of layer 2, k_s of layers 1 and 2, and the fraction of transpiration in evapotranspiration are sensitive (Fig. S6).

338 **4.3 Soil water content, chloride concentration and groundwater recharge**

339 Measured and simulated water content and chloride concentration profiles for individual scenarios are shown in Figure 6. The
340 average root mean squared error (RMSE) of simulated water content for all individual scenarios ranges from 0.02 to 0.06 cm^3
341 cm^{-3} (Table 4). In general, the models reproduce well the water content and chloride concentrations. However, the dynamics
342 of measured and simulated water contents differ considerably for ST1 and partly for ST2, although maximum values do match.
343 The models do not match the high chloride concentrations in the uppermost part of soil profiles for ST3, WL1, and WL2. The
344 standard deviations in chloride concentration of the randomly selected MVG model runs are exceptionally high in the lower part of



345 ST2 that corresponds to the poor sensitivity of the chloride concentration at the upper boundary and the comparably wide range
346 of measured chloride concentration in ponding water in the Salamat region ($2.5 \text{ mg l}^{-1} - 25 \text{ mg l}^{-1}$).

347 The interannual variability of modelled groundwater recharge differs considerably among locations (Figure 7, Table 5). In
348 general, interannual groundwater recharge variability depends on vegetation and soil texture with related water retention
349 capacity. Vegetation with deep roots on soil with comparably high water retention capacity have a stronger interannual
350 variability, e.g. at ST1, ST2 where recharge occurs only in years with high precipitation. Fine textured soils with shallow
351 rooting vegetation have an intermediate variability (WL1, WL2, and WL3), where years without recharge occur only during
352 drought periods. The coarser textured soils with grass cover have low interannual recharge variability (ST3) and recharge
353 occurs each year. Years with high precipitation, e.g. 2006, 2007, and 2008 in Waza Logone as well as 2010 in Salamat,
354 produced strong groundwater recharge.

355 The highest average annual recharge (93 mm) was calculated for ST3 in Salamat (Table 6), where the water balance during
356 the rainy season (July-September) is higher compared to the Waza Logone region, and where shallow rooting vegetation
357 prevails on comparably coarse soil texture with low water retention capacity and higher hydraulic conductivity. The other
358 locations in Salamat have lower calculated annual recharge, due to deep rooting vegetation and higher soil water retention
359 capacity. The impact of soil texture on annual groundwater recharge becomes apparent by comparing the three locations in
360 Waza Logone with the same vegetation on soils with different water retention capacities and hydraulic conductivities.
361 Groundwater recharge expressed as a fraction of precipitation is between 1% and 4% (Table 5), which is within the range of
362 0.1 to 5% published by Scanlon et al. (2006). Only at WL2 (8%) and ST3 (12%), where coarse soil textures enhance recharge,
363 a comparably high fraction is estimated.

364 Simulated chloride concentration and water budget of the soils over the simulated time-period are rather unstable and differ
365 for the six locations. At location ST2 with clay loam soil covered by Acacia and grass, accumulation of chloride takes place
366 over several years, due to the high transpiration related to the effective field capacity. However, in high precipitation years,
367 most of the accumulated chloride is leached to groundwater and soil concentration diminishes, which can be seen from the
368 time-varying differences of the cumulative solute fluxes between the top and bottom boundaries (Figure 8). The difference
369 between cumulative solute flux between the top and bottom boundaries represents the magnitude of chloride accumulation in
370 soil. It should be noted that at this site, the measured chloride concentrations cannot be reconstructed, if only input via
371 precipitation is considered. The measured profile can only be plausibly modelled with an additional input via ponding water.
372 Chloride input at the upper boundary is consequently six-times higher at ST2 compared to the other locations considered in
373 this study.

374 At location ST3, the chloride accumulation is much lower compared to the other locations. The chloride budget is controlled
375 by the fast groundwater recharge response to precipitation, which flushes chloride annually from the soil towards the
376 groundwater. Most of the chloride which infiltrated with precipitation remains in the vadose zone over several years and is
377 leached towards groundwater mainly during years with precipitation or water infiltration above threshold values (Figure 8).
378 Chloride accumulation is highest in profiles with clay soils and high effective field capacity (ST1, WL1, and WL3).



379 Chemical memory effects are subject to the dynamics of the water and chloride balance. Therefore, steady-state assumptions
380 are unsuitable. Accurate estimations are only possible with transient assumptions.

381 **4.4 Evaporation and transpiration**

382 The amount of transpiration depends on the availability of water in the root zone and the type of vegetation cover. At ST1,
383 annual transpiration presents two peaks: one related to sorghum and the other to grass (Figure 9). At each location and in every
384 simulation year, soil water content in the root zone reaches the wilting point defined by the specific parametrization of the root
385 water uptake model.

386 The actual evaporation rate depends mainly on the availability of water in the upper soil zone (Table 6). Clay and clay-loam
387 with relatively high water storativity have larger amounts of evaporated water compared to sand and loam soils. During dry
388 seasons, the uppermost part of the soils dries up annually, which significantly restricts evaporation.

389 Actual evapotranspiration is lower than the reference evapotranspiration most of the year. During and shortly after the rainy
390 season, when sufficient soil water is available, actual evapotranspiration is comparable to or higher than ET_0 depending on the
391 vegetation.

392 **5 Discussion**

393 Soil texture information is helpful to constrain the MVG parameter ranges while searching for realistic parameter sets
394 (Sprenger et al., 2015). However, poor representation of soil moisture dynamics using MVG parameters derived using Rosetta
395 are reported (Sprenger et al., 2015) suggesting that soil structure has to be taken into account (Vereecken et al., 2010),
396 especially for soils where high rock content influences water flow due to inherent heterogeneity (Sprenger et al., 2015). The
397 soils at the locations considered in this study belong to Quaternary sediments in the Lake Chad basin and heterogeneity due to
398 rock fragments is largely absent. Furthermore, soil moisture dynamics over the year are much higher in soils of the Waza
399 Logone floodplain compared to soils from the more humid regions in the south, where annual precipitation, although high,
400 occurs only over 4-5 months. It is expected that high soil moisture dynamics, rather homogeneous soils, and the monthly
401 resolution of climate data result in a minor impact of soil structure on MVG parametrization and groundwater recharge as
402 shown in Section 3.2. Soil moisture dynamics at all locations considered in this study are limited by water availability for
403 evaporation in the uppermost part of the soil and by water uptake in the root zone, but not by the reference evapotranspiration.
404 However, because time resolution of precipitation and evapotranspiration data is monthly, the models probably underestimate
405 soil moisture dynamics.

406 Calculated chloride concentrations for the soil profiles give indications of appropriate MVG parametrization as well as
407 evaporation and transpiration partitioning. However, uncertainty of chloride input and its transient variability in particular is
408 expressed in rather wide and partly bimodal distributions of the scaling factor (sc_{Conc}) included in the calibration (Figures
409 S1-S6 in supplement material). On one hand, measured chloride concentrations in precipitation are in agreement with other
410 studies in central Africa (Goni et al., 2001; Laouali et al., 2012; Gebru and Gebru and Tesfahunegn, 2019) and its transient



411 behaviour within the rainy season is considered in the applied model. On the other hand, impact of dry deposition is unknown,
412 because of data scarcity and potential lateral flow of periodic flooding. Furthermore, due to the monthly resolution of the
413 atmospheric boundary condition, extreme rain events that cause surface runoff cannot be reflected in the model. The variability
414 of chloride concentration in some of the soil profiles, which cannot be completely reproduced by the model, indicates either a
415 higher variability of chloride input and/or a larger variability in soil physics.

416 Bouchez et al. (2019) identified a chloride deficit between deposition and river export in the Chari-Logone river system of
417 88% (only 12% of the deposited chloride is exported via river water). They refer to the chemical memory effect, which can
418 play an important role in arid regions. Our simulations show the importance of the vadose zone for storage of chloride over
419 longer periods of time, which explains the fate of chloride in the basin and confirms the chemical memory effect. In this
420 context, it must be noted that the thickness of the vadose zone at the locations considered in this study is between 4 m and 21
421 m, where important amounts of chloride can be potentially stored leading to a strong delay of the chemical signal from
422 precipitation to groundwater.

423 In general, the calculated mean annual groundwater recharge values are within the ranges of 0.2 to 35 mm yr⁻¹ estimated by
424 Edmunds et al. (2002) using the CMB method in seven chloride profiles in northern Nigeria. The larger values (90 mm yr⁻¹ in
425 ST3 and 54 mm yr⁻¹ in WL2) are due to local coarse soil.

426 **6 Conclusions**

427 The quantitative estimation of groundwater recharge in the LCB is difficult due to the scarce data availability and the expected
428 low recharge quantities. Estimation of low recharge amounts in arid and semi-arid areas are usually ambiguous, because the
429 inherent measurement inaccuracies lead to uncertainties during data processing and modelling. Quantification of water and
430 solute fluxes in the vadose zone is often implemented using long-term time series of soil moisture, pressure heads, and
431 concentration data in combination with appropriate models. Monitoring of soil moisture and solute concentration over longer
432 periods at different depths and sites is difficult in the LCB, due to limited infrastructure and challenging climatic boundary
433 conditions. The presented approach combines soil moisture and chloride concentration quantified along vertical soil profiles
434 in different locations within the LCB with numerical models and freely accessible data, while considering data uncertainty.
435 Calculated chloride concentrations for the soil profiles provide appropriate MVG parametrization as well as evaporation and
436 transpiration partitioning. Although measured and simulated dynamic behaviour of both water contents and chloride
437 concentrations differ considerably in profiles ST1 and partly in ST2, their magnitudes largely agree. This is especially
438 important for chloride concentrations in the middle and deeper parts of the profiles, where seasonal effects are mainly averaged.
439 Thus, the estimates of soil water balance and especially of groundwater recharge as well as the adopted soil physical parameters
440 are plausible.

441 Mean groundwater recharge values estimated in this study are different than those published in Tewelde et al. (2019). This is
442 due to the more extensive availability of chloride concentration data in precipitation for this study. In addition, Tewelde et al.
443 (2019) roughly estimated one value of saturated porosity for each profile. This parameter is rather sensitive in the Bayesian



444 calibration and several values along each of the profiles were considered in this study. In contrast to the assessment of
445 groundwater recharge with the CMB (Tewolde et al., 2019), the method used here allows not only estimates of mean recharge,
446 but also its interannual dynamics, variability, and the classification of the uncertainties of the input data and modelling results.
447 The interannual variability of groundwater recharge is generally higher than the uncertainty of the modelled groundwater
448 recharge. The soil moisture dynamics at all locations considered in this study are limited by water availability for evaporation
449 in the uppermost part of the soil and by water uptake in the root zone and not by the reference evapotranspiration.
450 Simulations show the importance of the vadose zone for storage of chloride over longer time-periods and explain the fate of
451 chloride in the basin. The thickness of the vadose zone at the locations considered in this study varies between 4 m and 21 m.
452 Important amounts of chloride can be potentially stored significantly delaying the chemical signal from precipitation to
453 groundwater.
454 Upscaling of the results to larger areas must be interpreted with caution since the considered combinations of soils and
455 vegetation probably do not cover all combinations present in the Salamat and Waza Logone regions.

456 **Author contribution**

457 M.R. conducted fieldwork; A.G.M.S. and C.N. conducted modelling and interpretation; C.N. and S.V. designed the study and
458 completed the writing. All authors contributed to the discussion of results and commented on the manuscript.

459 **Acknowledgement**

460 This study was conducted within the framework of the technical cooperation project “Lake Chad Basin - Management of
461 Groundwater Resources” jointly executed by the Lake Chad Basin Commission (LCBC) and the German Federal Institute for
462 Geosciences and Natural Resources (BGR). The technical project is funded by the German Federal Ministry for Economic
463 Cooperation and Development (BMZ). We thank Daniel Tewolde, Paul Königer and Anna Degtjarev for their support in the
464 lab. We are highly indebted to John Molson for the thorough linguistic review of our manuscript.

465 **References**

466 Allen, R. G., Pereira, L. S., Dirk, R., and Smith, M.: Crop evapotranspiration: Guidelines for computing crop water
467 requirements. FAO Irrigation and Drainage Paper No. 56. Rome, Italy. <https://doi.org/10.1016/j.eja.2010.12.001>, 1998.
468 Alves, M. E. B., Mantovani, E. C., Sedyama, G. C., and Neves, J. C. L. (2013). Estimate of the crop coefficient for Eucalyptus
469 cultivated under irrigation during initial growth. *Cerne*, 19(2), 247–253. <https://doi.org/10.1590/s0104-77602013000200008>
470 Anderson, R. G., Zhang, X., and Skaggs, T. H.: Measurement and Partitioning of Evapotranspiration for Application to Vadose
471 Zone Studies. *Vadose Zone Journal*, 16(13), 0. <https://doi.org/10.2136/vzj2017.08.0155>, 2017
472 Aouade, G., Ezzahar, J., Amenzou, N., Er-Raki, S., Benkaddour, A., Khabba, S., and Jarlan, L.: Combining stable isotopes,
473 Eddy Covariance system and meteorological measurements for partitioning evapotranspiration, of winter wheat, into soil



- 474 evaporation and plant transpiration in a semi-arid region. *Agricultural Water Management*, 177, 181–192.
475 <https://doi.org/10.1016/J.AGWAT.2016.07.021>, 2016.
- 476 Bader, J., Lemoalle, J., and Leblanc, M.: Modèle hydrologique du Lac Tchad, *Hydrolog. Sci. J.*, 56, 411–425, 2011.
- 477 Batello, C., Marzot, M., and Harouna Touré, A.: The future is an ancient lake: Traditional knowledge, biodiversity and genetic
478 resources for food and agriculture in the Lake Chad basin ecosystems. FAO Interdepartmental Working Group on Biological
479 Diversity for Food and Agriculture, Rome, 2004.
- 480 Bernacsek, G. M., Hughes, J. S., and Hughes, R. H. (Ed.): A directory of African wetlands. International Union for the
481 Conservation of Nature and Natural Resources, 1992.
- 482 Beyer, M., Koeniger, P., and Himmelsbach, T.: Constraining water uptake depths in semi-arid environments using stable water
483 isotopes Results & Discussion. <https://doi.org/10.5281/zenodo.56159>, 2016.
- 484 Bouchez, C., Deschamps P., Goncalves J., Hamelin, B., Nour, A.M., Vallet-Coulomb C., and Sylvestre, F: Water transit time
485 and active recharge in the Sahel inferred by bomb-produced ^{36}Cl . *Nature, scientific reports*, 9: 7465, (2019).
- 486 Bouchez, C., Goncalves, J., Deschamps, P., Vallet-Coulomb, C., Hamelin, B., Doumnang, J.C., Sylvestre, F.: Hydrological,
487 chemical, and isotopic budgets of Lake Chad: a quantitative assessment of evaporation, transpiration and infiltration fluxes,
488 *Hydrol. Earth Syst. Sci.*, 20, 1599–1619, 2016.
- 489 Carmouze, J.-P.: Originalité de la régulation saline du lac Tchad, *Comptes Rendus de l'Académie des Sciences. Série D:*
490 *Sciences Naturelles*, 275, 1871–1874, 1972.
- 491 Cuthbert, M. O., Taylor, R.G., Favreau, G. et al.: Observed controls on resilience of groundwater to climate variability in sub-
492 Saharan Africa. *Nature*, 572: 230-234, <https://doi.org/10.1038/s41586-019-1441-7>, 2019.
- 493 Didan, K.: MOD13Q1 MODIS/Terra Vegetation Indices 16-Day L3 Global 250m SIN Grid V006. NASA EOSDIS Land
494 Processes DAAC. <https://doi.org/10.5067/MODIS/MOD13Q1.006>, 2015.
- 495 Didane, D. H., Rosly, N., Zulkafli, M. F., and Shamsudin, S. S.: Evaluation of wind energy potential as a power generation
496 source in Chad. *International Journal of Rotating Machinery*, vol. 2017, Article ID 3121875, 10 pp, 2017.
- 497 Do, F. and Rocheteau, A.: Cycle annuel de transpiration d'Acacia raddiana par la mesure des flux de sève brute (Nord-Sénégal).
498 In *Un arbre au désert: Acacia raddiana* (pp. 119–142). Paris, (2003).
- 499 Do, F. C., Rocheteau, A., Diagne, A. L., Goudiaby, V., Granier, A., and Lhomme, J. P.: Stable annual pattern of water use by
500 *Acacia tortilis* in Sahelian Africa. *Tree Physiology*, 28(1), 95–104. <https://doi.org/10.1093/treephys/28.1.95>, 2008.
- 501 Edmunds, W. M. and Gaye, C.B.: Estimating the spatial variability of groundwater recharge in the Sahel using chloride. *J.*
502 *Hydrol.*, 156(1-4):47-59, 1994.
- 503 Edmunds, W. M., Fellman, E., and Goni, I. B.: Spatial and temporal distribution of groundwater recharge in northern Nigeria.
504 *Hydrogeology Journal*, 10:205-215, 2002.
- 505 Feddes, R. A., Kowalik, P. J., and Zaradny, H.: Simulation of field water use and crop yield. Published in 1978 in Wageningen
506 by Centre for agricultural publishing and documentation. Wageningen: Centre for Agricultural Pub. and Documentation.
507 <https://lib.ugent.be/catalog/rug01:000032129>, 1978.



- 508 Fontes, J.-C., Maglione, G., and Roche, M.-A.: Données isotopiques préliminaires sur les rapports du lac Tchad avec les nappes
509 de la bordure nord-est, Cah. Orstom. Hydrobiol., 6, 17– 34, 1969.
- 510 Fontes, J.-C., Gonfiantini, R., and Roche, M.-A. : Deuterium et oxygène-18 dans les eaux du Lac Tchad. Isotope Hydrology,
511 IAEA-SM-129/23, 1970.
- 512 Gebru, T.A. and Tesfahunegn, G.B.: Chloride mass balance for estimation of groundwater recharge in a semi-arid catchment
513 of northern Ethiopia. Hydrogeology Journal, 27:363-378, 2019.
- 514 Global Soil Data Task Group: Global Gridded Surfaces of Selected Soil Characteristics (IGBP-DIS). ORNL DAAC, Oak
515 Ridge, Tennessee, USA. <https://doi.org/10.3334/ORNLDAAC/569>, 2000.
- 516 Goni, I., Fellman, E., and Edmunds, W.: Rainfall geochemistry in the Sahel region of northern Nigeria, Atmos. Environ., 35,
517 4331– 4339, 2001.
- 518 Groh, J., Stumpp, C., Lücke, A., Pütz, T., Vanderborght, J., and Vereecken, H.: Inverse estimation of soil hydraulic and
519 transport parameters of layered soils from water stable isotopes and lysimeter data, Vadose Zone Journal 17:170168.
520 Doi:10.2136/vzj2017.09.0168, 2018.
- 521 Gröning, M., Lutz, H.O., Roller-Lutz, Z., Kralik, M., Gourcy, L., Pölsenstein, L.: A simple rain collector preventing water re-
522 evaporation dedicated for $\delta^{18}\text{O}$ and $\delta^2\text{H}$ analysis of cumulative precipitation samples. J. Hydrol. 448-449, 195-200, 2012.
- 523 Harris, I., Osborn, T. J., Jones, P. and Lister, D.: Version 4 of the CRU TS monthly high-resolution gridded multivariate
524 climate dataset. Sci Data 7, 109 (2020) <https://doi.org/10.1038/s41597-020-0453-3>.
- 525 Isihoro, S., Matisoff, G., and Wehn, K.: Seepage relationship between Lake Chad and the Chad Aquifers, Groundwater, 34,
526 819– 826, 1996.
- 527 Hartig, F., Minunno, F., Paul, S.: BayesianTools: General-Purpose MCMC and SMC Samplers and Tools for Bayesian
528 Statistics, 2019.
- 529 Jasechko, S., Sharp, Z. D., Gibson, J. J., Birks, S. J., Yi, Y., and Fawcett, P. J.: Terrestrial water fluxes dominated by
530 transpiration, Nature, 496, 347–350, 2013.
- 531 Kool, D., Agam, N., Lazarovitch, N., Heitman, J. L., Sauer, T. J., and Ben-Gal, A.: A review of approaches for
532 evapotranspiration partitioning. Agricultural and Forest Meteorology, 184, 56–70, 2014.
- 533 Lake Chad Basin Commission. (1993). Monitoring and management of groundwater resources in the Lake Chad Basin.
534 Mapping of aquifers, water resources management, final report, R35985, Report BRGM R 35985 EA U/4S/93.
- 535 Lake Chad Basin Commission. (2012). Report on the State of the Lake Chad Basin Ecosystem.
536 http://www.cbtl.org/sites/default/files/download_documents/report_on_the_state_of_the_lake_chad_basin_ecosystem.pdf.
- 537 Laouali, D., Galy-Lacaux, C., Diop, B., Delon, C., Orange, D., Lacaux, J.P., Akpo, A., Lavenu, F., Gardrat, E., Castera, P.,
538 2012. Long term monitoring of the chemical composition of precipitation and wet deposition fluxes over three Sahelian
539 savannas. Atmos. Environ. 50, 314–327. <https://doi.org/10.1016/j.atmosenv.2011.12.004>
- 540 Leblanc, M.: Gestion des ressources en eau des grands bassins semi-arides à l'aide de la télédétection et des SIG: application
541 à l'étude du bassin du lac Tchad, Afrique, PhD thesis, Université de Poitiers, Poitiers, 2002.



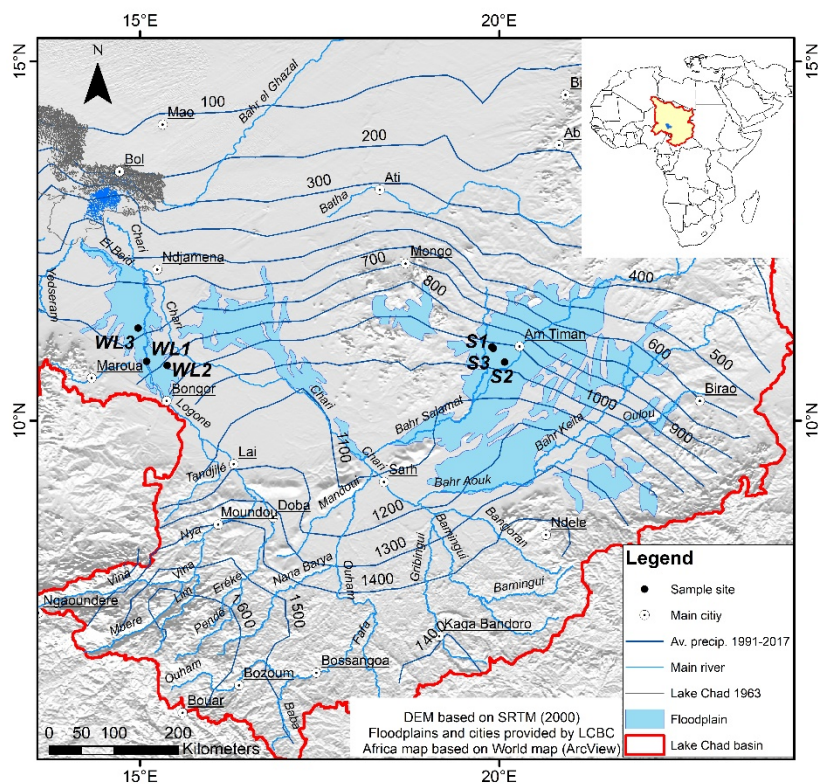
- 542 Leblanc, M., Favreau, G., Tweed, S., Leduc, C., Razack, M., and Mofor, I.: Remote sensing for groundwater modelling in
543 large semiarid areas: Lake Chad basin, Africa. *Hydrogeology Journal*, 15(1), 97-100, 2007.
- 544 Lemoalle, J., Bader, J.-C., Leblanc, M., and Sedick, A.: Recent changes in Lake Chad: observations, simulations and
545 management options (1973–2011), *Global Planet. Change*, 80, 247–254, 2012.
- 546 Lloyd, J. W.: A review of aridity and groundwater, *Hydrological Processes*, Vol. 1, 63-78, 1986.
- 547 Lloyd, J. W.: Groundwater in arid and semiarid regions. In: Silveira, L. and Usunoff E.J. [Eds.]: *Groundwater (Vol. I)*,
548 *Encyclopedia of Life Support Systems*, pp. 284–307, 2009.
- 549 Majnooni-Heris, A., Sadraddini, A. A., Nazemi, A. H., Shakiba, M. R., Neyshaburi, M. R., and Tuzel, I. H.: Determination of
550 single and dual crop coefficients and ratio of transpiration to evapotranspiration for canola. *Annals of Biological Research*,
551 3(4), 1885–1894, 2012.
- 552 Mertens, J., Barkle, G. F., and Stenger, R.: Numerical analysis to investigate the effects of the design and installation of
553 equilibrium tension plate lysimeters on leachate volume, *Vadose Zone Journal*, 4:488-499, 2005.
- 554 Millington, R. J. and Quirk, J. P.: Permeability of porous solids. *Trans. Int. Congr. Soil Sci.*, 7(1), 97-106, 1961.
- 555 Mualem, Y.: A new model for predicting the hydraulic conductivity of unsaturated porous media, *Water Resour. Res.*, 12,
556 513–522, doi:10.1029/WR012i003p00513, 1976.
- 557 Ngatcha, B. N., Mudry, J., and Leduc, C.: The state of understanding on groundwater recharge for the sustainable management
558 of transboundary aquifer in the Lake Chad basin, 2008.
- 559 Olivry, J., Chouret, A., Vuillaume, G., Lemoalle, J., and Bricquet, J.: *Hydrologie du lac Tchad*, Editions de l'ORSTOM, Paris
560 1996.
- 561 Richards, L. A.: Capillary conduction of liquids through porous mediums. *Physics*, 1(5), 318-333, 1931.
- 562 Righes, A. A.: Water uptake and root distribution of soybeans, grain sorghum and corn. *Retrospective Theses and*
563 *Dissertations*. Iowa State University, 1980.
- 564 Roche, M.: Tracage naturel salin et isotopique des eaux du système du Lac Tchad, These de Doctorat d'Etat, Travaux et
565 Documents de l'ORSTOM, ORSTOM (Office de la Recherche Scientifique et Technique d'Outre-Mer) editions, Paris, 1980.
- 566 Scanlon, B. R., Keese, K. E., Flint, A. L., Flint, L. E., Gaye, C. B., Edmunds, W. M., and Simmers, I.: Global synthesis of
567 groundwater recharge in semiarid and arid regions. *Hydrol. Process.* 20, 3335-3370, 2006.
- 568 Schaap, M. G., Leij, F. J., and van Genuchten, M. T.: ROSETTA: a computer program for estimating soil hydraulic parameters
569 with hierarchical pedotransfer functions, *Journal of Hydrology*, 251, 163-176, 2001.
- 570 Schenk, H. J. and Jackson, R. B.: Rooting depths, lateral root spreads and belowground aboveground allometries of plants in
571 water limited ecosystems. *Journal of Ecology*, 90, 480–494. <https://doi.org/10.1046/j.1365-2745.2002.00682.x>, 2002.
- 572 Shahrokhnia, M. H. and Sepaskhah, A. R.: Single and dual crop coefficients and crop evapotranspiration for wheat and maize
573 in a semi-arid region. *Theoretical and Applied Climatology*, 114(3–4), 495–510. <https://doi.org/10.1007/s00704-013-0848-6>,
574 2013.



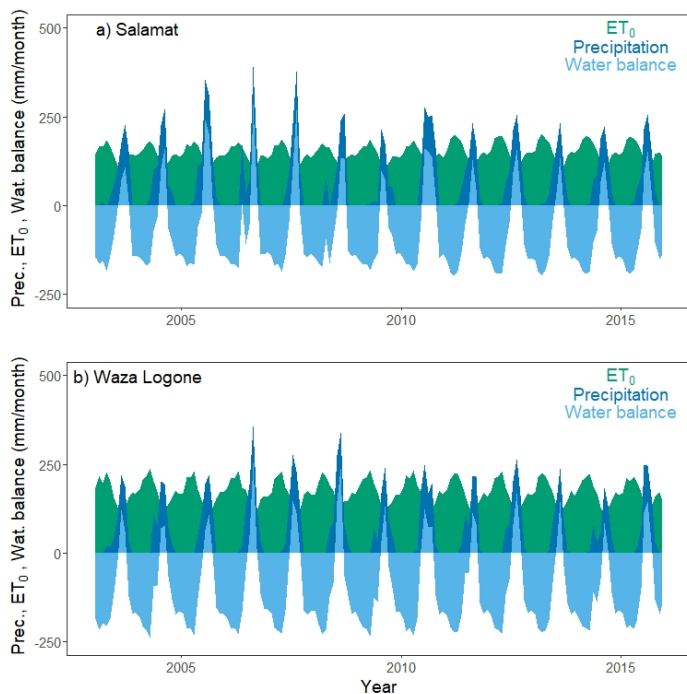
- 575 Šimůnek, J., Sejna, M., Saito, H., Sakai, M., and van Genuchten, M. Th.: The HYDRUS-1D software package for simulating
576 the one-dimensional movement of water, heat, and multiple solutes in variably-saturated media, Version 4.15, Riverside,
577 California, 2009.
- 578 Šimůnek, J., Šejna, M., & van Genuchten, M. T.: The HYDRUS Software Package for Simulating the Two- and Three-
579 Dimensional Movement of Water, Heat, and Multiple Solutes in Variably-Saturated Media. Prague, 2011.
- 580 Sprenger, M., Volkmann, T. H. M., Blume, T., and Weiler, M.: Estimating flow and transport parameters in the unsaturated
581 zone with pore water stable isotopes, *Hydrol. Earth Syst. Sci.*, 19(6), 2617-2635, doi:10.5197/hess-19-2617-2015, 2015.
- 582 Stumpp, C., Nützmann, G., Maciejewski, S., and Maloszewski, P.: A comparative modeling study of a dual tracer experiment
583 in a large lysimeter under atmospheric conditions, *Journal of Hydrology*, 375, 566-577, 2009.
- 584 Stumpp, C., Stichler, W., Kandolf, M., and Šimůnek, J.: Effects of land cover and fertilization method on water flow and solute
585 transport in five lysimeters: a long-term study using stable water isotopes, *Vadose Zone Journal*, 11(1), doi:
586 10.2136/vzj2012.0075, 2012.
- 587 ter Braak, C.J.F., Vrugt, J.A.: Differential Evolution Markov Chain with snooker updater and fewer chains. *Stat. Comput.* 18,
588 435–446. <https://doi.org/10.1007/s11222-008-9104-9>, 2008.
- 589 Tewolde, D. O.: Investigating unsaturated zone water transport processes by means of biogeochemical analysis of soil depth
590 profiles: a comparative study of two semi-arid sites. M.Sc.-Thesis, Leibniz Universitaet Hannover, 2017.
- 591 Tewolde, D. O., Koeniger, P., Beyer, M., Neukum, C., Gröschke, M., Ronnelngar, M., Rieckh, H., and Vassolo, S.: Soil water
592 balance in the Lake Chad Basin using stable water isotope and chloride of soil profiles. *Isot. Environ. Health Stud.* 55, 459-
593 477. <https://doi.org/10.1080/10256016.2019.1647194>, 2019.
- 594 Tong, G. D., Liu, H. L., and Li, F. H.: Evaluation of dual crop coefficient approach on evapotranspiration calculation of cherry
595 trees. *International Journal of Agricultural and Biological Engineering*, 9(3), 29–39.
596 <https://doi.org/10.3965/j.ijabe.20160903.1886>, 2016.
- 597 Vanderborght, J. and Vereecken, H.: Review of dispersivity for transport modeling in soils, *Vadose Zone Journal*, 6(1), 29-52,
598 doi:10.2136/vzj2006.0096, 2007.
- 599 van Genuchten, M. T.: A close-form equation for predicting the hydraulic conductivity of unsaturated soils 1, *Soil Science*
600 *Society of America Journal*, 8(44), 892-898, 1980.
- 601 van Looy, K., Bouma, J., Herbst, M., Koestel, J., Minasny, B., Mishra, U., Montzka, C., Nemes, A., Pachepsky, Y. A.,
602 Padarian, J., and Schaap, M. G.: Pedotransfer functions in earth system science: challenges and perspectives, *Reviews of*
603 *Geophysics*, 55(4), 1199-1256, doi: 10.1002/2017RG000581, 2017.
- 604 Vassolo, S.: The aquifer recharge and storage systems to reduce the high level of evapotranspiration. In: *Adaptive Water*
605 *Management in the Lake Chad Basin. World Water Week 09, FAO*, pp. 30-44, 2009.
- 606 Vereecken, H., Javaux, M., Weynants, M., Pachepsky, Y. A., Schaap, M. G., and van Genuchten M. T.: Using pedotransfer
607 functions to estimate the van Genuchten-Mualem soil hydraulic properties: A review, *Vadose zone Journal*, 9(4), 759-820,
608 doi: 10.2136/vzj2010.0045, 2010.



609 Vereecken, H., Schnepf, A., Hopmans, J. W., Javaux, M., Or, D., Roose, T., ... and Young, I. M.: Modeling soil processes:
610 Review, key challenges, and new perspectives, *Vadose Zone Journal*, 15(5), 1-57, doi: 10.2136/vzj.2015.09.0131, 2016.
611 Vieira, P. V. D., de Freitas, P. S. L., Ribeiro da Silva, A. L. B., Hashiguti, H. T., Rezende, R. and Junior, C. A. F.: Determination
612 of wheat crop coefficient (K_c) and soil water evaporation (K_e) in Maringa, PR, Brazil, *African Journal of Agricultural*, 11(44),
613 4551–4558. <https://doi.org/10.5897/AJAR2016.11377>, 2016.
614 Vuillaume, G.: Bilan hydrologique mensuel et modélisation sommaire du régime hydrologique du lac Tchad, *Cahiers*
615 *ORSTOM. Série Hydrologie*, 18, 23–72, 1981.
616 Wu, Y., Du, T., Ding, R., Tong, L., and Li, S.: Multiple Methods to Partition Evapotranspiration in a Maize Field. *Journal of*
617 *Hydrometeorology*, 139–149. <https://doi.org/10.1175/JHM-D-16-0138.1>, 2016.
618 Zairi, R.: Étude géochimique et hydrodynamique du Bassin du Lac Tchad (la nappe phréatique dans les régions du Kadzell
619 (Niger oriental) et du Bornou (Nord-Est du Nigéria)), PhD thesis, Université de Montpellier 2, Montpellier, 2008.
620



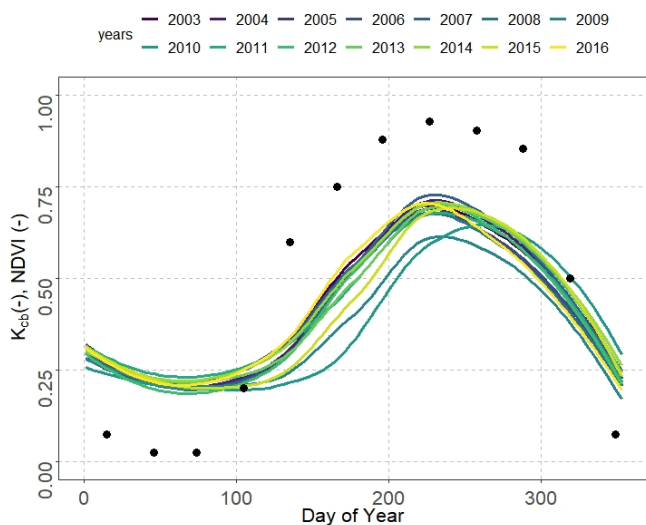
621
622 **Figure 1: Location of the six soil sampling sites within the Logone and Salamat river basins in the Lake Chad catchment. The map**
623 **inset shows the location of the Lake Chad basin in Africa.**



624

625 **Figure 2: Monthly precipitation, reference evapotranspiration from the CRUTS 4 database (NCAR, 2017) and derived water balance**
 626 **for Salamat and Waza Logone.**

627

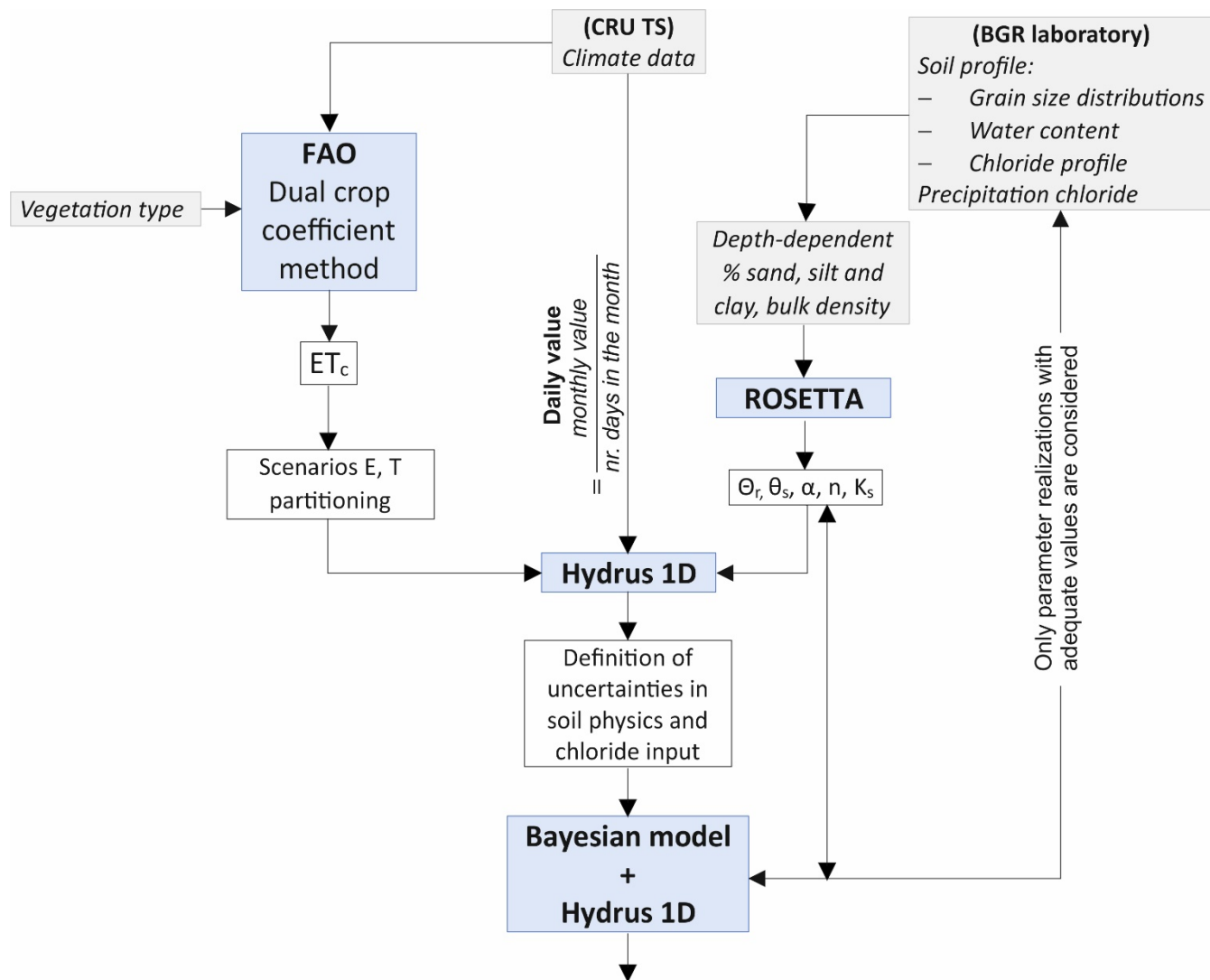


628

629 **Figure 3: Average Normalized Difference Vegetation Index (NDVI, MODIS 16 day interval and 250 m spatial resolution) measured**
 630 **between 2003 and 2016 in the Salamat region and estimated monthly basal crop coefficient (K_{cb} , black points) for location S3.**

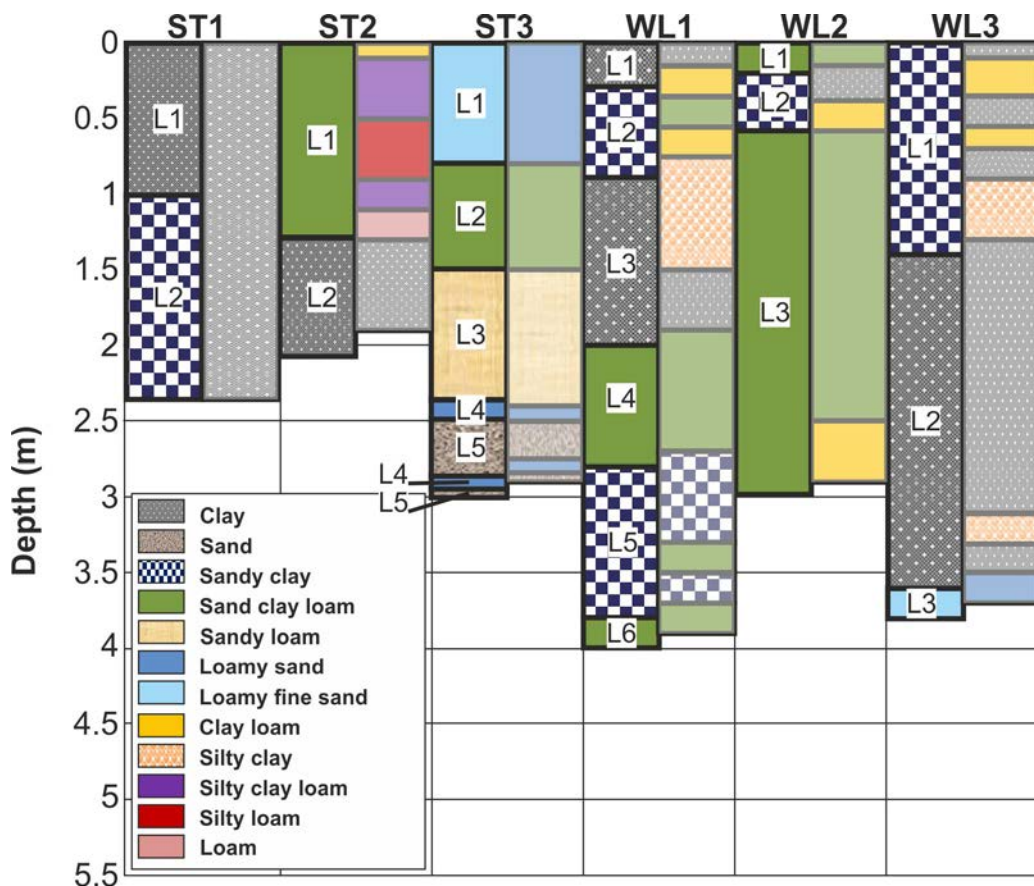
631

632



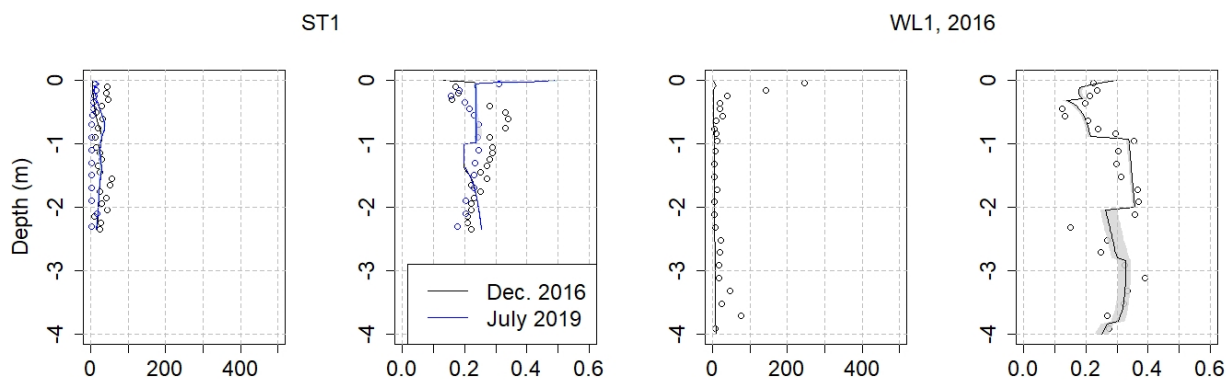
633

634 **Figure 4: Workflow of the modelling activities**

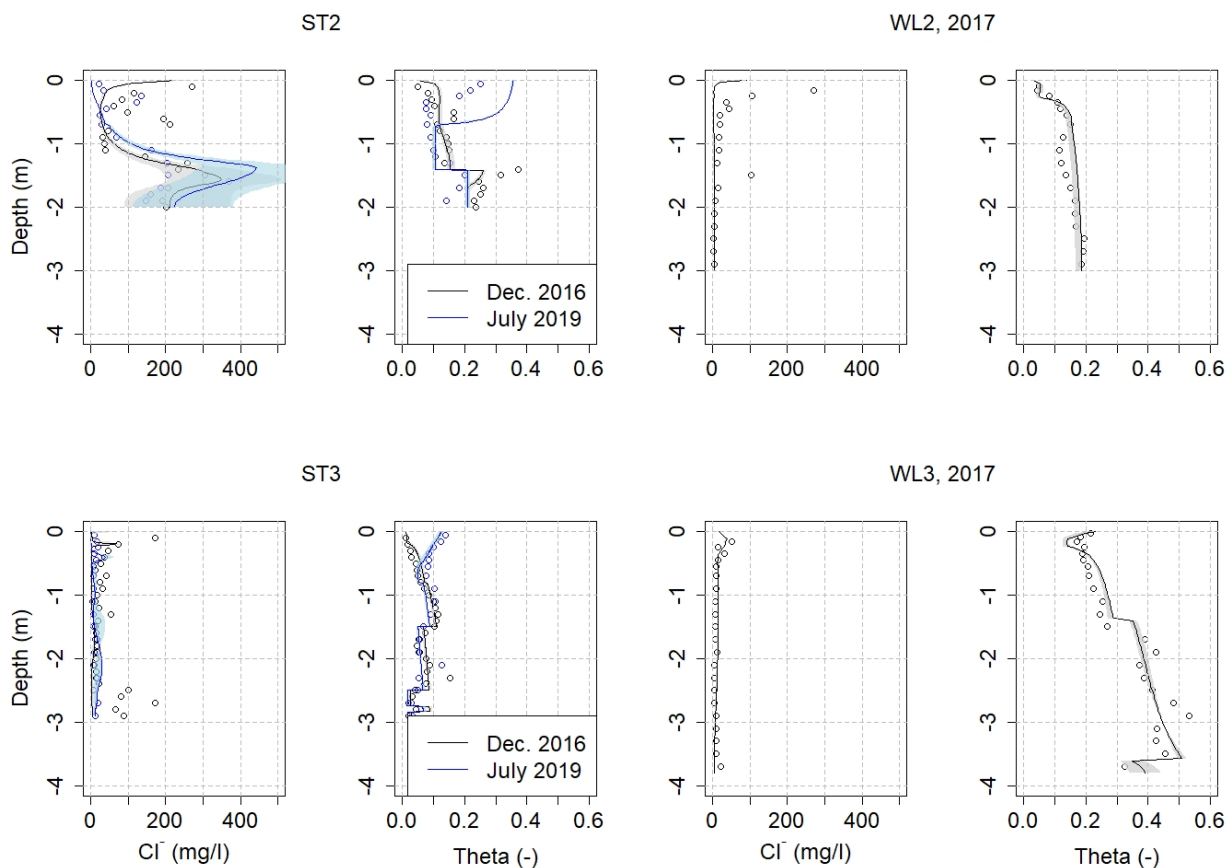


635

636 **Figure 5: Soil textures used in the model (left column) defined according to the grain size distribution analysis (right column) for**
 637 **each of the six soil profiles.**



638

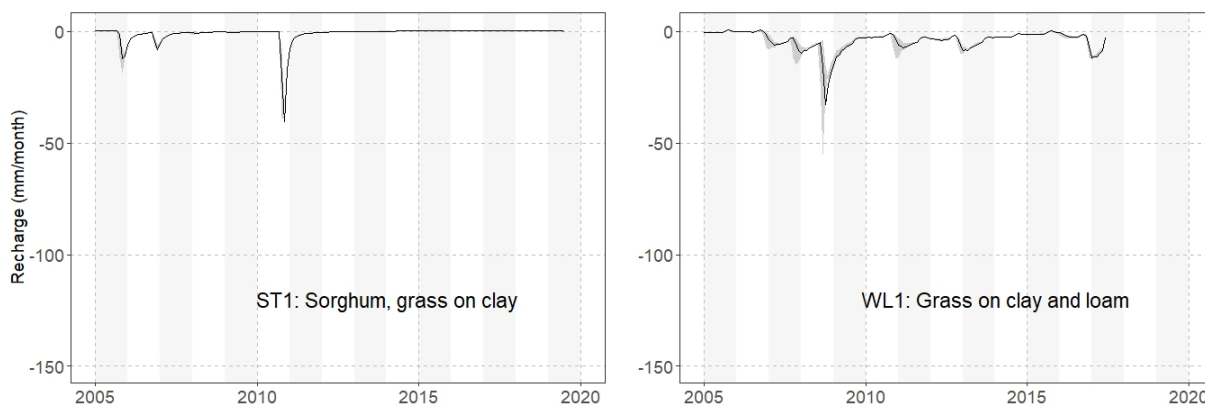


639

640

641 **Figure 6: Measured and simulated scenarios of chloride concentration and water content for all six soil profiles. Shaded areas**
 642 **represent the standard deviation of 100 randomly selected model runs.**

643



644

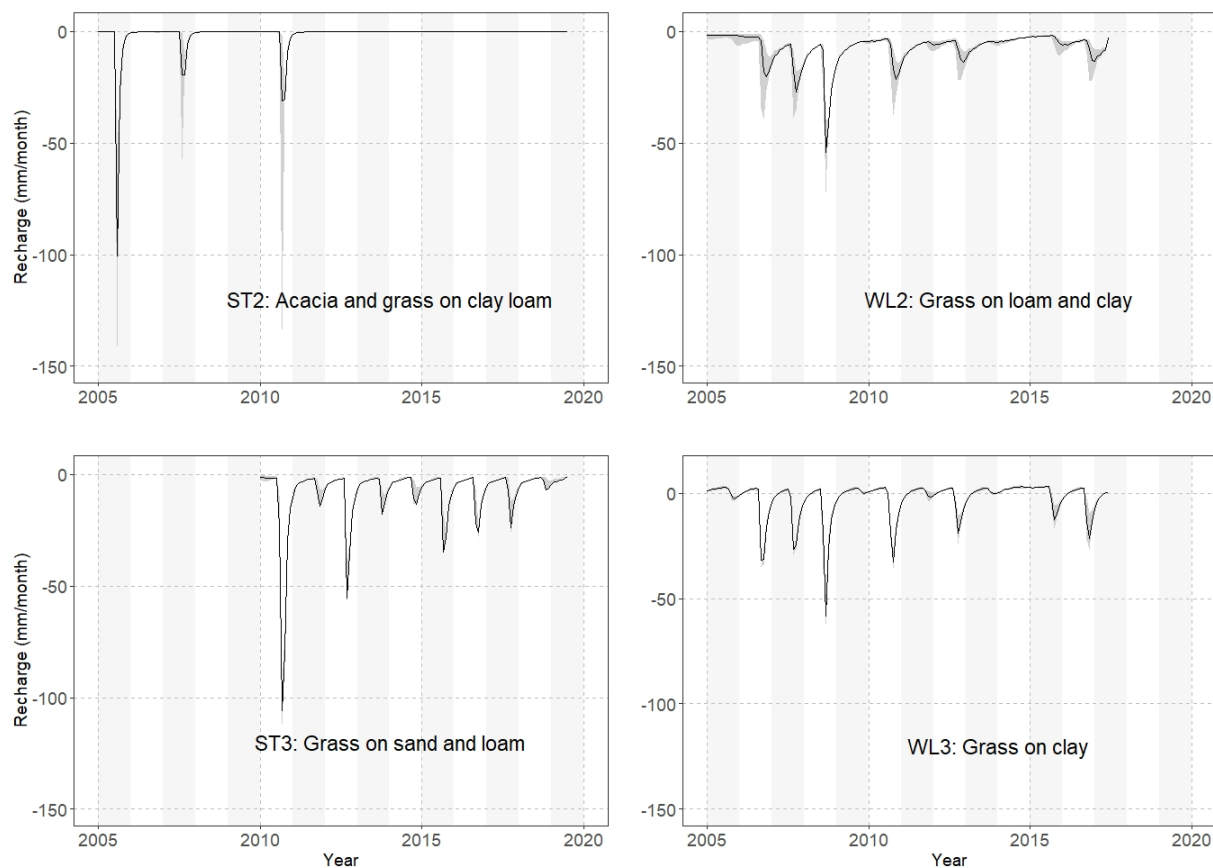
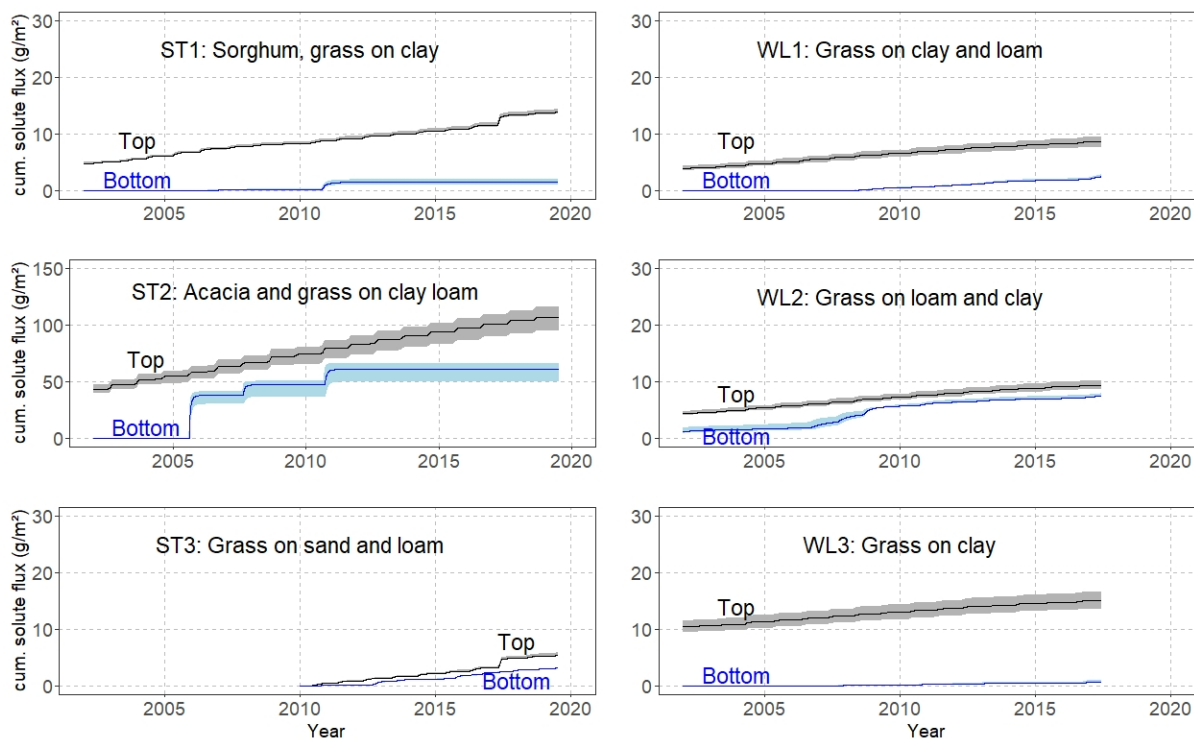


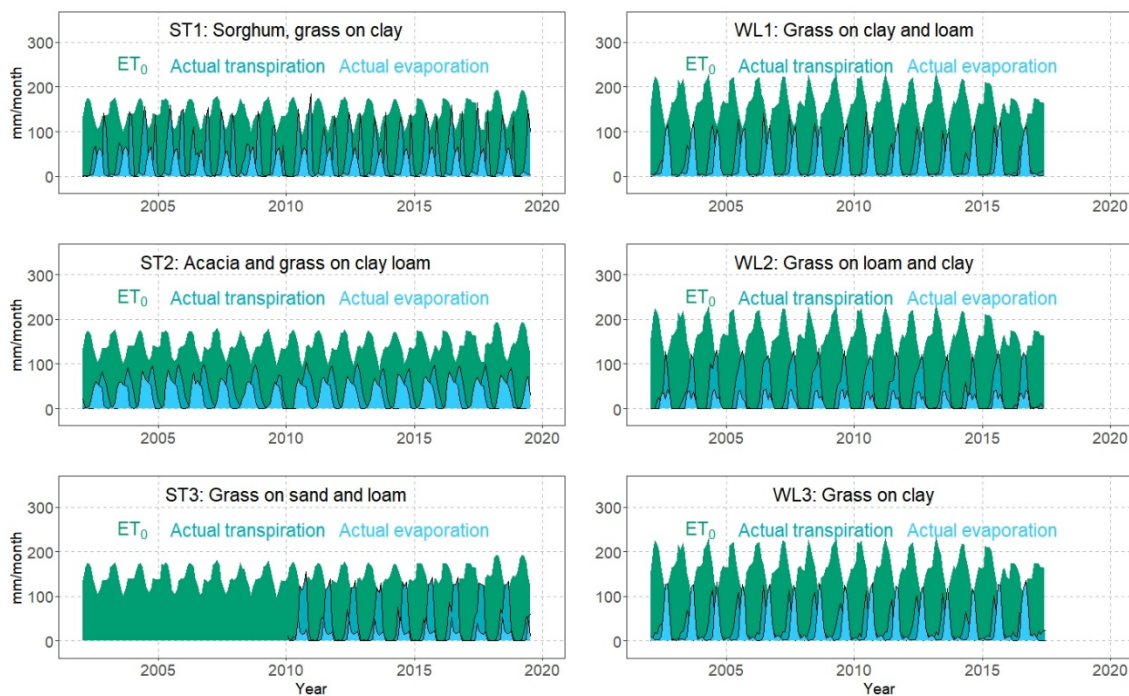
Figure 7: Calculated groundwater recharge for all scenarios and sampling locations with indication of vegetation and soil texture.



648

649 **Fig. 8: Cumulative solute flux on the upper and lower boundary of the models. The shaded areas represent the standard deviation**
650 **of 100 randomly selected model runs. Note the different y-axis scales between sites.**

651



652

653 **Fig. 9:** Reference evapotranspiration from the CRUTS 4 database (NCAR 2017) as well as modelled average actual evaporation and
 654 transpiration of 100 randomly selected model runs.

655

656 **Table 1:** Names and geographic coordinates of the sampling locations with average depths to groundwater.

Name	Location	Date of Sampling	Drilling depth (m)	Longitude (°)	Latitude (°)	Elevation (m a.s.l.)	Depth to Groundwater (m)
ST1	Gos	07-12-2016	2.35	19.89644	11.02582	418	21
	Djarat	11-07-2019	5.0				
ST2	Kach	09-12-2016	2.0	20.07473	10.81649	396	16-18
	Kacha	16-07-2019	5.0				
ST3	Gos	11-12-2016	2.2	19.91687	11.00629	418	21
	Djarat	13-07-2019	5.0				
WL1	Katoa	01-06-2017	4.0	15.09235	10.82508	362	4
WL2	Loutou	01-06-2017	3.0	15.37817	10.76805	325	11-12
WL3	Zina	08-06-2017	3.8	14.97363	11.28858	304	3.6

657



658 **Table 2: Crop evapotranspiration scenarios used with the individual soil profiles.**

Scenario	K_{cb}	K_e	Root depth	Profile
Mean	average	average	average	All profiles
Min	minimum	minimum	average	All profiles
Min-RD	minimum	minimum	minimum	WL1
Mix-1	minimum	average	average	All profiles
Mix-2	average	minimum	average	ST1, WL2, WL3
Mix-3	maximum	average	average	ST3
Max	maximum	maximum	average	All profiles

659

660 **Table 3: Parametrization of water retention and unsaturated hydraulic conductivity functions according the Mualem-van**
 661 **Genuchten model after Bayesian model calibration.**

Location	Texture	Depth (m)	θ_r (-)	θ_s (-)	α (m ⁻¹)	n (-)	k_s (md ⁻¹)
ST1	Clay	0-1	0.001	0.61±0.01	2.13±0.27	1.164±0.008	0.09±0.14
	Sandy clay	1-2.35	0.04	0.43±0.03	2.63±0.37	1.150±0.011	0.43±0.39
ST2	Sandy clay loam	0-1.4	0.04	0.38±0.02	1.18±0.08	1.36±0.047	0.03±0.16
	Clay	1.4 -2.1	0.07	0.48±0.08	2.66±0.36	1.203±0.052	0.11±0.28
ST3	Loamy fine sand	0-0.8	0.01	0.45±0.08	3.69±0.08	2.332±0.196	2.96±5.72
	Sandy clay loam	0.8-1.5	0.043	0.38±0.07	2.81±0.43	2.210±0.172	2.44±4.19
	Sandy loam	1.5-2.4	0.02	0.43±0.08	3.44±0.51	2.469±0.330	1.66±2.84
ST3	Loamy sand	2.4-2.5	0	0.35±0.06	3.77±0.53	1.980±0.265	2.03±3.11
	Sand	2.5-2.75	0	0.34±0.04	3.73±0.53	2.730±0.372	5.42±8.86
	Loamy sand	2.75-2.84	0	0.35±0.06	3.77±0.53	1.980±0.265	2.03±3.11
	Sand	2.84-2.9	0	0.34±0.04	3.73±0.53	2.730±0.372	5.42±8.86
WL1	Clay	0-0.3	0.065	0.56±0.09	1.37±0.19	1.293±0.092	0.17±0.26
	Sandy clay	0.3-0.9	0.06	0.44±0.07	2.85±0.36	1.416±0.125	0.21±0.38
	Clay	0.9-2.0	0.103	0.42±0.03	1.55±0.21	1.187±0.065	0.19±0.42
	Sandy clay loam	2.0-2.8	0.075	0.49±0.07	2.34±0.33	1.598±0.227	0.13±0.28
	Sandy clay	2.8-3.8	0.081	0.43±0.06	2.60±0.35	1.266±0.134	0.09±0.19



	Sandy clay loam	3.8-4.0	0.071	0.40±0.05	2.69±0.37	1.291±0.137	0.12±0.24
	Sandy clay loam	0-0.2	0.03	0.41±0.07	3.22±0.45	1.502±0.151	0.30±0.57
WL2	Sandy clay	0.2-0.6	0.01	0.37±0.06	2.56±0.39	1.422±0.081	0.09±0.19
	Sandy clay loam	0.6-3.0	0.01	0.37±0.03	1.39±0.19	1.566±0.06	0.10±0.10
	Sandy clay	0-1.4	0.09	0.49±0.09	1.27±0.15	1.470±0.111	0.22±0.14
WL3	Clay	1.4-3.6	0.105	0.53±0.05	2.03±0.29	1.285±0.100	0.17±0.36
	Loamy fine sand	3.6-3.8	0.056	0.39±0.08	2.90±0.45	1.789±0.293	1.23±2.40

662

663 **Table 4: Average root mean square error (RMSE) and related standard deviation (SD) over all scenarios for water content (Theta)**
 664 **and chloride concentration.**

Location, Year	Theta (cm ³ cm ⁻³)			Chloride concentration (mg l ⁻¹)		
	Average observation	Average simulation	Average RMSE	Average observation	Average simulation	Average RMSE
ST1, 2016/2019	0.25/0.22	0.23/0.23	0.06/0.04	30/6	18/22	19/19
ST2, 2016/2019	0.17/0.14	0.16/0.15	0.06/0.04	162/106	132/229	82/116
ST3, 2016/2019	0.06/0.08	0.07/0.06	0.02/0.02	42/10	6/13	58/10
WL1, 2017	0.27	0.27	0.05	31	6	59
WL2, 2017	0.13	0.15	0.02	40	3	117
WL3, 2017	0.31	0.33	0.04	12	13	9

665

666 **Table 5: Calculated average annual recharge, fraction of recharge on average annual precipitation, standard deviations of recharge**
 667 **across the time-period 2005-2019 and 2005 – 2016 for Salamat and Waza Logone, respectively.**

Location	Average annual recharge (mm)	Fraction of average annual precipitation (%)	Standard deviation of annual recharge (mm)
ST1	7	0.9	17
ST2	9	1	29
ST3	93	12	69
WL1	28	4	32
WL2	54	8	46
WL3	6	1	48



668 **Table 6: Calculated average annual evaporation and transpiration and related standard deviations of 100 randomly accepted model**
669 **runs.**

Location	Average annual evaporation (mm)	Standard deviation of evaporation (mm)	Average annual transpiration (mm)	Standard deviations of transpiration (mm)	Average actual evapotranspiration (mm)
ST1	210	9	553	11	763
ST2	366	22	388	27	754
ST3	137	12	552	11	689
WL1	344	20	317	23	661
WL2	146	14	477	28	623
WL3	376	12	305	10	681

670